NANO LETTERS

Letter

pubs.acs.org/NanoLett

A Silicon Electromechanical Photodetector

Siddharth Tallur and Sunil A. Bhave*

OxideMEMS Lab, Cornell University, Ithaca 14850, New York, United States

ABSTRACT: Optomechanical systems have enabled wide-band optical frequency conversion and multichannel all-optical radio frequency amplification. Realization of an on-chip silicon communication platform is limited by photodetectors needed to convert optical information to electrical signals for further signal processing. In this paper we present a coupled silicon microresonator, which converts near-IR optical intensity modulation at 174.2 MHz and 1.198 GHz into motional electrical current. This device emulates a photodetector which detects intensity modulation of continuous wave laser light in the full-width-at-half-maximum bandwidth of the mechanical resonance. The resonant principle of operation eliminates dark current challenges associated with convetional photodetectors. While the results presented here constitute a purely classical demonstration, the device can also potentially be extended to the quantum regime to realize a photon−phonon translator.

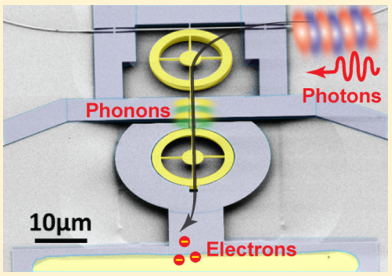

KEYWORDS: *Optomechanics, silicon photodetector, optical gradient force, electromechanical capacitive sense, photon−phonon translator, integrated optics*

Cavity optomechanical systems offer a unique platform wherein the coherent interaction rate is larger than the thermal decoherence rate of the system, as realized in ground-state cooling experiments.[1] This interplay of light and motion opens up an array of novel applications in classical and quantum optics communication.[2−4] In the classical regime, optomechanical systems have enabled wide-band optical frequency conversion[5] and multichannel all-optical radio frequency amplification.[6] Realization of an on-chip silicon communication platform is limited by photodetectors needed to convert optical information to electrical signals for further signal processing.

Classical and quantum information transfer and storage utilize photons for long-range communication.[7−9] Photons are appealing for such applications on account of their weak interaction with the environment and resiliency to thermal noise due to their high frequency. On the other hand, acoustic phonons have lower bandwidth and experience significantly higher losses associated with transmission but can be delayed and stored for longer times and can interact resonantly with RF-microwave electronic systems. It has been proposed in the past that a hybrid phononic−photonic system could perform a range of tasks unreachable by purely photonic and phononic systems.[10−12] Furthermore, such a system should also be capable of being directly integrated with electronics used for processing radio frequency (RF) signals. Recent research efforts have enabled the realization of optomechanical systems where photons are used to manipulate mechanical vibrations and vice versa.[12−17] Achieving this in an all silicon chip-scale platform has been pursued with great zest, as silicon processing offers benefits in terms of lowering manufacturing cost, obtaining high yields, and promises seamless on-chip integration with electronics. However, as the field of silicon photonics has grown, a theme that has emerged is that, as a platform, silicon does not provide best-in-class devices for all tasks.[18] True monolithic integration of photonics devices with cutting-edge 28 nm or smaller CMOS processes is a very challenging task. Making process modifications to support such integration will fundamentally change the models for transistors, at the cost of degrading their performance. Not modifying the process is an option, and recently researchers have shown that some photonic functionality can be integrated with minimal postprocessing in a silicon-on-insulator (SOI) CMOS process.[19] A key component for CMOS compatible silicon photonics is a photodiode capable of detecting light in the near-infrared region. Various CMOS compatible photodiodes have been demonstrated,[20−23] but they suffer from complex processing steps to overcome lattice mismatch issues, large area consumption, and susceptibility to dark current. Here, we present an alternate photodetector that responds optomechanically to optical intensity modulation. The device is comprised of a silicon microresonator designed in a CMOS silicon-on-insulator (SOI) platform, which converts optical intensity modulation into motional electrical current, thus converting the signal from photon→phonon→electron, instead of depending on an avalanche or photoelectric process in a nonsilicon material. This scheme is universal and could potentially be of interest to optomechanical resonators fabricated in piezoelectric materials such as aluminum nitride[24,25] and materials with attractive mechanical and optical properties such as single crystalline diamond.[26] The experiments and theoretical analysis presented in this paper constitute a purely classical demonstration of converting optical modulation to an RF electronic signal. The device we present here can, in principle, enable quantum state transfer as proposed in other optomechanical systems.[10,27]

Received: March 15, 2013
Revised: May 15, 2013
Published: May 24, 2013

dx.doi.org/10.1021/nl400980u | *Nano Lett.* 2013, 13, 2760−2765

Figure 1 shows an illustration showcasing the principle of operation of this detector. The device is comprised of two

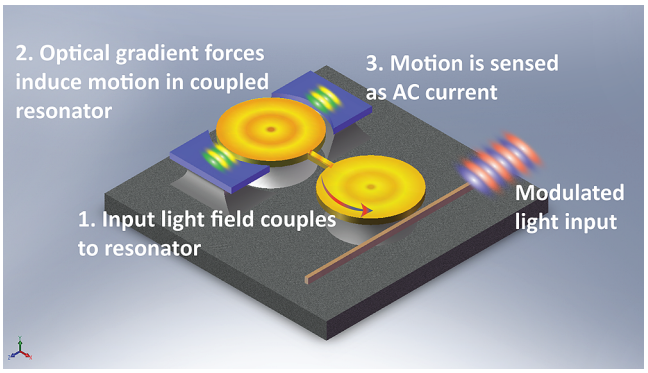

Figure 1. Illustration of operation of the electromechanical photodetector.

mechanical resonators that are coupled to each other via a mechanical beam. The resonator that is located in close proximity to the waveguide serves as an optomechanical resonator and is actuated via optical gradient forces generated by the modulated input light field. These mechanical vibrations $\tilde{x}(\Omega)$ are coupled to the other mechanical resonator flanked by electrodes via the coupling beam. The motion of this resonator is sensed via a high dynamic range electrostatic capacitive sense scheme, resulting in an AC current ($\tilde{i}_{out}(\Omega)$) generated on account of modulation of the capacitance formed by the air gap between the resonator and the electrode.

Consider an input pump field $A_p(t) = A_{p0}(t) + \delta A_p(t)$, where the first term denotes static field amplitude and the second term is a dynamic modulated term. Correspondingly the intracavity dropped field can be expressed similarly as $a_p(t) = a_{p0}(t) + \delta a_p(t)$, where:

$$a_{p0} = \frac{j\sqrt{\Gamma_{ex}}}{(\Gamma_{tot}/2) - j\Delta_p} A_{p0} \tag{1}$$

Here Δ_p is the detuning of the laser (ω_p) from the cavity resonance (ω_0), and Γ_{in}, Γ_{ex}, and Γ_{tot} are the intrinsic cavity photon decay rate, photon decay rate associated with coupling to the cavity, and photon decay rate of the loaded optical cavity, respectively. The intracavity field is normalized to the intracavity energy, $U_p = |a_p|^2$. The optical gradient force acting on the optomechanical resonator can then be expressed as follows:[28]

$$F_{grad} = -\frac{g_{OM} U_p}{\omega_p} \tag{2}$$

g_{OM} denotes the optomechanical coupling coefficient. The gradient force consists of two terms: $F_{grad}(t) = F_{grad,0}(t) + \delta F_{grad}(t)$. The first term is a static force whereas the second term is the dynamic component related to the laser light modulation $\delta U_p(t)$, given by:

$$\delta F_{grad}(t) = -\frac{g_{OM}\delta U_p}{\omega_p} = -\frac{g_{OM}}{\omega_p}[a_{p0}^* \delta a_p(t) + a_{p0}\delta a_p^*(t)] \tag{3}$$

The mechanical motion (x) of the cavity follows: $\ddot{x} + \Gamma m\dot{x} + \Omega_m{}^2 x = [F_{grad,0}(t) + \delta F_{grad}(t) + F_T]/m_{eff}$, where m_{eff} is the effective mass of the mechanical mode with frequency Ω_m, Γ_m is the intrinsic mechanical damping rate, and F_T is the thermal Langevin force responsible for the thermal Brownian motion. The dynamic displacement of the resonator is affected largely by the dynamic gradient force, as the thermal Langevin force is relatively much smaller in magnitude. The back-action of the mechanical motion changes the value of the resonant frequency and damping rate of mechanical motion. The spectral response of this force is given by:[28]

$$f_0(\Omega) = -\frac{2g_{OM}^2 U_{p0}\Delta_p}{\omega_p} \times \frac{\Delta_p^2 - \Omega^2 + (\Gamma_{tot}/2)^2 + j\Gamma_{tot}\Omega}{[(\Delta_p + \Omega)^2 + (\Gamma_{tot}/2)^2][(\Delta_p - \Omega)^2 + (\Gamma_{tot}/2)^2]} \tag{4}$$

Define $l(\Omega) = \Omega_m^2 - \Omega^2 - j\Gamma_m\Omega - (f_o(\Omega)/m_{eff})$. The dynamic mechanical displacement on account of the optical gradient force is given by:

$$\tilde{x}(\Omega) = \frac{j\sqrt{\Gamma_{ex}}g_{OM}}{m_{eff}\omega_p l(\Omega)} \times \left[\frac{a_{p0}^*\delta\tilde{A}_p(\Omega)}{j(\Delta_p + \Omega) - (\Gamma_{tot}/2)} + \frac{a_{p0}\delta\tilde{A}_p^*(-\Omega)}{j(\Delta_p - \Omega) + (\Gamma_{tot}/2)}\right] \tag{5}$$

Here $\delta\tilde{A}_p$ is the Fourier domain representation of the modulated input light field. This expression is complete in the sense that it accounts for motion actuated due to the optical gradient force acting on the resonator and also the back-action induced by the motion on the optical field. Substituting eq 1 into eq 5 yields:

$$\tilde{x}(\Omega) = \frac{-\Gamma_{ex}g_{OM}}{m_{eff}\omega_p l(\Omega)[(\Gamma_{tot}/2) - j\Delta_p]} \times \left[\frac{A_{p0}^*\delta\tilde{A}_p(\Omega)}{j(\Delta_p + \Omega) - (\Gamma_{tot}/2)} + \frac{A_{p0}\delta\tilde{A}_p^*(-\Omega)}{j(\Delta_p - \Omega) + (\Gamma_{tot}/2)}\right] \tag{6}$$

In the unresolved sideband regime, the equation above reduces to the limit $\lim_{\Omega\to 0}\tilde{x}(\Omega)$:

$$\tilde{x}(\Omega) = \{ - \Gamma_{ex}g_{OM}[-j\Delta_p(A_{p0}^*\delta\tilde{A}_p(\Omega) + A_{p0}\delta\tilde{A}_p^*(-\Omega)) - (\Gamma_{tot}/2)(A_{p0}^*\delta\tilde{A}_p(\Omega) - A_{p0}\delta\tilde{A}_p^*(-\Omega))]\} /\{m_{eff}\omega_p l(\Omega)((\Gamma_{tot}/2) - j\Delta_p)[\Delta_p^2 + (\Gamma_{tot}^2/4)]\} \tag{7}$$

$$\tilde{x}(\Omega) \approx \frac{-\Gamma_{ex}g_{OM}[-j\Delta_p(A_{p0}^*\delta\tilde{A}_p(\Omega) + A_{p0}\delta\tilde{A}_p^*(-\Omega))]}{m_{eff}\omega_p l(\Omega)((\Gamma_{tot}/2) - j\Delta_p)[\Delta_p^2 + (\Gamma_{tot}^2/4)]} \tag{8}$$

$$\tilde{x}(\Omega) = \frac{j\Delta_p\Gamma_{ex}g_{OM}\delta P_{in}(\Omega)}{m_{eff}\omega_p l(\Omega)((\Gamma_{tot}/2) - j\Delta_p)[\Delta_p^2 + (\Gamma_{tot}^2/4)]} \tag{9}$$

The derivation above assumes that the displacement amplitude of the resonator is small; that is, the perturbation of the detuning on account of mechanical motion is very small

dx.doi.org/10.1021/nl400980u | Nano Lett. 2013, 13, 2760−2765

compared to the unperturbed detuning $[(x(t)/R)\omega_0 \ll \Delta_p]$. In the large amplitude regime, where the detuning oscillates between large positive and negative values, the small signal model derived above fails to hold. An extensive study of optomechanical oscillation amplitudes was recently presented by Poot et al.[29] The optical backaction on the resonator enables radiation pressure induced self-sustained oscillations whose limit cycle is set by the dynamic range of the cavity. This sets a maximum limit on the amplitude of mechanical motion,[29] which would amount to the saturation of the motional current generated by the detector.

If C denotes the capacitance formed by the air gap between the resonator and the electrode, and g denotes the resonator-electrode gap, the motional current flowing into the electrode in response to the motion of the resonator and applied DC voltage, V_{dc} is expressed as:

$$i_{out}(t) = V_{dc}\frac{dC}{dt} = V_{dc}\frac{dC}{dg}\frac{dg}{dt} \tag{10}$$

the dynamic component of this current can then be written down as:

$$\tilde{i}_{out}(\Omega) = V_{dc}\frac{dC}{dg}j\Omega\tilde{x}(\Omega) = V_{dc}\frac{\varepsilon_0 Rh\theta}{g^2}j\Omega\tilde{x}(\Omega) \tag{11}$$

Here R, h, and θ denote the outer radius of the resonator, device thickness, and the electrode−resonator overlap angle, respectively. Substituting eq 9 into eq 11, we get:

$$\frac{\tilde{i}_{out}(\Omega)}{\delta P_{in}(\Omega)} = \frac{-\Delta_p\Gamma_{ex}g_{OM}V_{dc}\varepsilon_0 Rh\theta\Omega}{g^2 m_{eff}\omega_p l(\Omega)((\Gamma_{tot}/2) - j\Delta_p)[\Delta_p^2 + (\Gamma_{tot}^2/4)]} \tag{12}$$

The expression derived above in eq 12 can be interpreted as the "electromechanical responsivity" ($\mathcal{R}_{em}$) of the detector.

We choose a coupled microring geometry[14] for the photodetector. The motional current amplitude varies as inverse-square of the resonator−electrode gap (g) as shown in eq 12, and hence it is desirable to reduce the gap to boost the detection efficiency. The smallest gaps that we could define were limited by the resolution of lithography, and hence the gap is set to 50 nm in our device to enable efficient electrostatic transduction. The outer radius (R) of the ring resonators is 9.5 μm, and the silicon device layer thickness (h) is 220 nm. As evident from eq 12, the greater the electrode overlap angle (θ), higher the current measured. The coupling spring forces us to leave a 10° opening in the electrode where it connects to the sense resonator. To maintain symmetry of design and ensure mechanical momentum balance we introduce another 10° opening on the diametrically opposite section of the electrode, as seen in the scanning electron micrograph (SEM) in Figure 2.

Fabricating the photodetector involves a four mask process flow on a custom silicon-on-insulator (SOI) wafer (undoped 250 nm device layer for low optical loss and 3 μm thick buried oxide for isolation of the waveguides on device layer from the silicon substrate). The top silicon is thermally oxidized to obtain a thin oxide hard mask layer of thickness 60 nm atop a 220 nm thick silicon device layer. A ma-N 2403 electron beam resist is spun on top of the oxide and patterned using electron beam lithography. The patterns are transferred into the silicon dioxide using a CHF_3/O_2 based reactive ion etcher and then into the silicon device layer using a chlorine based reactive ion etch. A layer of SPR-220 3.0 photoresist is spun, and a second mask is used to pattern windows above the mechanical resonator, the electrical routing beams, and the bond-pads. This is followed by a boron ion implantation and nitrogen annealing to reduce the resistivity of these structures. A third mask is then used to deposit metal over the bond pads for improved electrical contact. A layer of LOR-5A followed by a layer of SPR-220 3.0 is spun, and the bond pads are exposed via contact alignment photolithography. This is followed by evaporation of 25 nm nickel on the sample. Nickel forms a good ohmic contact with silicon and is hence chosen as the bottommost metal. After evaporating nickel, we evaporate 25 nm titanium and 50 nm platinum. Platinum is used as the top metal as it makes good electrical contact with the Cascade air coplanar probe (ACP) RF probe used to interrogate these devices. However platinum does not adhere well to nickel, and hence titanium is used as an adhesion layer. The photoresist is dissolved in Microposit remover solvent 1165 to leave metal only atop bond-pads. A fourth mask is used to pattern release windows near the resonator using SPR-220 3.0 photoresist, followed by a timed release etch in buffered oxide etchant to undercut the devices. The samples are then dried using a critical point dryer to prevent stiction.

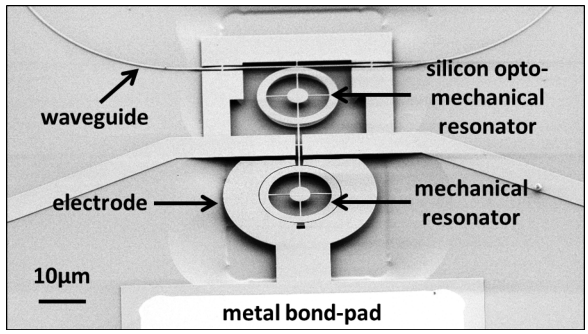

Figure 2. Scanning electron micrograph of the silicon electro-mechanical detector integrated with electrodes and a waveguide. The lithographically defined gap between the electrode and resonator is 50 nm.

Figure 3 shows a schematic of the experimental setup used to characterize the photodetector performance. Light from a Santec TSL-510 tunable diode laser is modulated with a Photline MXAN-LN-10 lithium niobate electro-optic intensity modulator (EOM). An Agilent N5230A network analyzer is used to characterize the detector efficiency. The input laser light is modulated by connecting the RF input of the modulator to port 1 of the network analyzer. The output power is sensed by connecting the signal from the metal bond pad to port 2 of the network analyzer.

The silicon optomechanical resonator has many optical resonances in the C-band as seen in Figure 4a. For the purpose of this experiment we choose an overcoupled resonance at 1548.9 nm, with an extinction of 8 dB shown in Figure 4b. As derived in eq 12, the motional current amplitude is proportional to the cavity coupling rate, Γ_{ex}, and hence operating with an overcoupled resonance is desirable. However, this also reduces the loaded optical quality factor, and hence there is a trade-off associated with overcoupling to the resonator. The rich optical spectrum of the resonator offers us a wide choice of optical resonances to choose from.

A DC bias voltage of 40 V is applied at the metal bond pad using a bias tee. We apply an input RF power ($P_{in,RF}$) of 0 dBm at port 1 of the network analyzer and measure the output RF

dx.doi.org/10.1021/nl400980u | Nano Lett. 2013, 13, 2760−2765

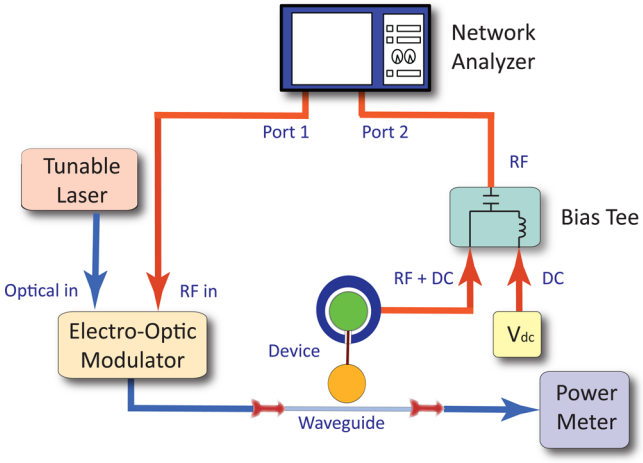

Figure 3. Schematic of the experimental setup used to characterize the silicon detector. Mechanical motion is actuated by modulating continuous wave laser light coupled into the optomechanical resonator using a Photline MXAN-LN-10 electro-optic modulator. The mechanical motion is sensed via electrostatic capacitive actuation by applying V_{dc} = 40 V DC voltage at the electrode using a bias tee. A network analyzer is used to measure the two-port transmission of the device.

power (P_{out}) at port 2. The transmission of the device operated in this configuration corresponds to the "gain" of the photodetector ($P_{out}/P_{in,RF}$). Figure 5 shows the measured gain for the detector at various input laser power levels measured at the resonator (by discounting the coupling loss). The signals measured correspond to mechanical vibrations of the fundamental radial expansion mode at 174.2 MHz and compound radial expansion mode at 1.198 GHz (panels a and b, respectively). The measured gain depends on the input laser power, akin to nanomechanical resonator based microwave amplification reported by Massel et al.[2]

The maximum laser power is set 4 dB below the threshold for onset of radiation pressure induced self-oscillations of the fundamental radial expansion mode. Measurements were carried out at room temperature and 5 mTorr pressure. The minimum detectable signal at the sense port of the network analyzer (port 2) is set by the receiver's noise floor at this port, which depends on the averaging factor used while carrying out the measurement. An averaging factor of 16 was used in all of the measurements to optimize the sensitivity of the network analyzer. The RF power applied at port 1 of the network analyzer is 0 dBm. The input laser wavelength is set to the 3 dB off resonance wavelength, and the laser is blue detuned with respect to the optical cavity. Measurements were carried out at room temperature and a pressure of 5 mTorr. The measured mechanical quality factors at 174.2 MHz and 1.198 GHz are 8700 and 6300, respectively. Substituting all of the experimental parameters into eq 11 and calculating the output power, $P_{out} = (|i_{out}|^2 R/2)$, where R = 50 Ω is the load resistance, yields a conversion gain of −97 dB at 174.2 MHz and −98 dB at 1.198 GHz for +9 dBm input laser power. The simulated gain at frequencies near 174.2 MHz and 1.198 GHz are shown in Figure 5c and d, which closely match measured gain values. The shift of the mechanical resonance frequency with increasing input laser power is attributed to thermal heating of the device due to absorption of light coupled into the optical cavity. Native single crystal silicon resonators have a negative temperature coefficient of frequency (TCF), and hence a larger optical power coupling into the cavity lowers the mechanical resonance frequency. This shift in frequency is negligibly small compared to the intrinsic mechanical resonance frequency ($\Delta\Omega_m/\Omega_m$) ∼ 0.1%), and hence this effect is not taken into account in simulation.

The conversion of signal from photons to phonons results in a conversion loss of Ω_m/ω_p, which is to be expected, as evident in eq 12. The loss values at 174.2 MHz and 1.198 GHz are −60 dB and −52 dB, respectively. Gaining insights from eq 12, one could envisage a detector design with larger gain that benefits from higher optical quality factor (Q_{tot}) resonances, smaller resonator−electrode gaps (g), and smaller detuning (Δ_p). However, choosing a smaller detuning value could potentially launch the device into radiation pressure induced self-oscillations,[29] which leads to amplitude saturation.

In conclusion, we have demonstrated an on-chip electromechanical detector fabricated on a CMOS SOI platform. The electromechanical sense scheme constitutes a high dynamic range detection medium, and we observe efficient signal detection at 174.2 MHz all the way up to 1.198 GHz. The mechanical resonance frequencies of this device are lithographically defined. The resonant nature of this scheme makes this device a narrow-band detector, whose bandwidth is limited by the quality factor of the mechanical resonance. The sense scheme is universal and can also be used for detection of optical modulation induced by radiation pressure vibrations, which has successfully been demonstrated at GHz rates in silicon.[24] This electromechanical detector thus introduces a valuable component in the library of existing novel optomechanical devices. To

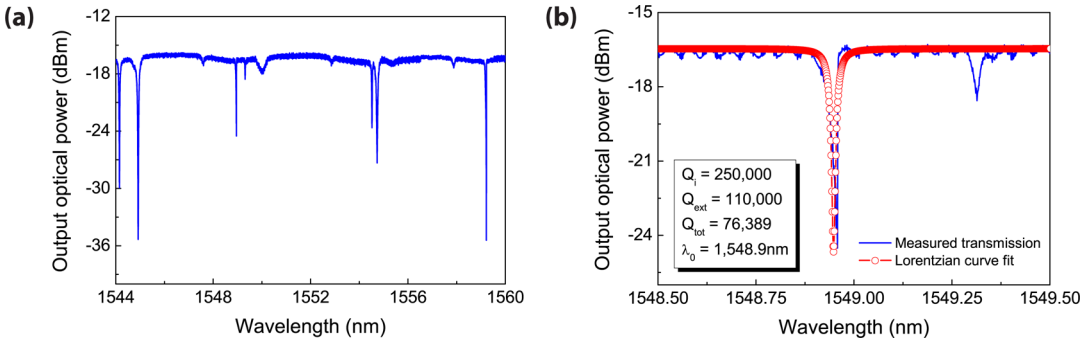

Figure 4. (a) Optical spectrum for the opto-mechanical resonator based silicon photodetector. The input laser power is +2 dBm. The connectors and grating couplers add 8 dB loss at each facet. (b) High optical Q resonance used to operate the photodetector. We intentionally choose an overcoupled resonance in order to measure larger motional current.

dx.doi.org/10.1021/nl400980u | Nano Lett. 2013, 13, 2760−2765

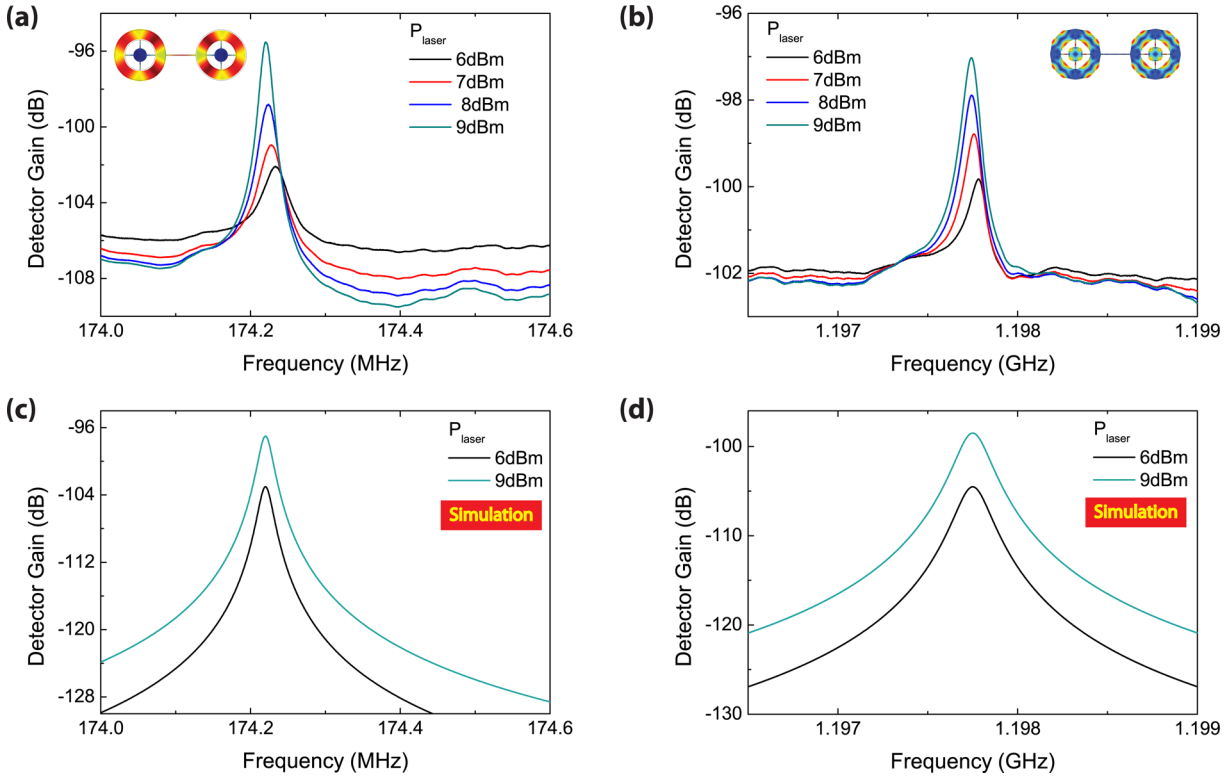

Figure 5. Frequency spectra for the detector gain ($P_{out}/P_{in,RF}$) measured using network analyzer. Measured detection of optical modulation for (a) fundamental radial expansion mode at 174.2 MHz and (b) compound radial expansion mode at 1.198 GHz. The insets in panels a and b show the corresponding finite element method (FEM) simulated mechanical mode-shapes. (c) Simulated transmission at frequencies near the fundamental radial expansion resonance frequency for laser power = +6 dBm and +9 dBm. (d) Simulated transmission at frequencies near the compound radial expansion resonance frequency for laser power = +6 dBm and +9 dBm. Simulations for expected gain are based on eq 11. Measurements were carried out at room temperature and a pressure of 5 mTorr.

the best of our knowledge, this constitutes the first experimental demonstration of a photon-to-phonon translator.

AUTHOR INFORMATION

Corresponding Author

*E-mail: sunil@ece.cornell.edu.

Notes

The authors declare no competing financial interest.

ACKNOWLEDGMENTS

The authors would like to acknowledge DARPA/MTO's ORCHID program for research support.

REFERENCES

(1) Chan, J.; Alegre, T. P. M.; Safavi-Naeini, A. H.; Hill, J. T.; Krause, A.; Grob-lacher, S.; Aspelmeyer, M.; Painter, O. *Nature* **2011**, *478*, 89−92.

(2) Massel, F.; Heikkila, T. T.; Pirkkalainen, J.-M.; Cho, S. U.; Saloniemi, H.; Hako-nen, P. J.; Sillanpaa, M. A. *Nature* **2011**, *480*, 351−354.

(3) Brooks, D. W. C.; Botter, T.; Schreppler, S.; Purdy, T. P.; Brahms, N.; Stamper-Kurn, D. M. *Nature* **2012**, *488*, 476−480.

(4) Dong, C.; Fiore, V.; Kuzyk, M. C.; Wang, H. *Science* **2012**, *338* (6114), 1609−1613.

(5) Hill, J. T.; Safavi-Naeini, A. H.; Chan, J.; Painter, O. *Nat. Commun.* **2012**, *3*, 1196.

(6) Li, H.; Chen, Y.; Noh, J.; Tadesse, S.; Li, M. *Nat. Commun.* **2012**, *3*, 1091.

(7) Agrawal, G. P. *Fiber-optic communication systems*, 3rd ed.; Wiley-Interscience: New York, 2012.

(8) Duan, L.-M.; Lukin, M. D.; Cirac, J. I.; Zoller, P. *Nature* **2001**, *414*, 413−418.

(9) Chaneliere, T.; Ruggiero, J.; Bonarota, M.; Afzelius, M.; Le Gouet, J.-L. *New J. Phys.* **2010**, *12*, 023025.

(10) Safavi-Naeini, A. H.; Painter, O. *New J. Phys.* **2011**, *13*, 013017.

(11) Davanco, M.; Chan, J.; Safavi-Naeini, A. H.; Painter, O.; Srinivasan, K. *Opt. Express* **2012**, *20* (22), 24394−24410.

(12) Eichenfield, M.; Chan, J.; Camacho, R. M.; Vahala, K. J.; Painter, O. *Nature* **2009**, *462*, 78−82.

(13) Carmon, T.; Rokhsari, H.; Yang, L.; Kippenberg, T. J.; Vahala, K. J. *Phys. Rev. Lett.* **2005**, *94*, 223902.

(14) Sridaran, S.; Bhave, S. A. *Opt. Express* **2011**, *19*, 9020−9026.

(15) Lee, K. H.; McRae, T. G.; Harris, G. I.; Knittel, J.; Bowen, W. P. *Phys. Rev. Lett.* **2010**, *104*, 123604.

(16) Yao, J.; Leuenberger, D.; Lee, M.-C. M.; Wu, M. C. *IEEE J. Sel. Top. Quantum Electron.* **2007**, *13*, 202−208.

(17) Perahia, R.; Cohen, J. D.; Meenehan, S.; Alegre, T. P. M.; Painter, O. *Appl. Phys. Lett.* **2010**, *19*, 191112.

(18) Baehr-Jones, T.; Pinguet, T.; Guo-Qiang, P. L.; Danziger, S.; Prather, D.; Hochberg, M. *Nat. Photonics* **2012**, *6*, 206−208.

(19) Orcutt, J. S.; Moss, B.; Sun, C.; Leu, J.; Georgas, M.; Shainline, J.; Zgraggen, E.; Li, H.; Sun, J.; Weaver, M.; Uroseciv, S.; Popovic, M.; Ram, R. J.; Stojanovic, V. *Opt. Express* **2012**, *20* (11), 12222−12232.

(20) Geis, M. W.; Spector, S. J.; Grein, M. E.; Yoon, J. U.; Lennon, D. M.; Lyszczarz, T. M. *Opt. Express* **2009**, *17* (7), 5193−5204.

(21) Preston, K.; Lee, Y. H. D.; Zhang, M.; Lipson, M. *Opt. Lett.* **2011**, *36* (1), 52−54.

(22) DeRose, C. T.; Trotter, D. C.; Zortman, W. A.; Starbuck, A. L.; Fisher, M.; Watts, M. R.; Davids, P. S. *Opt. Express* **2011**, *19* (25), 24897−24904.

(23) Michel, J.; Liu, J.; Kimerling, L. C. *Nat. Photonics* **2010**, *4*, 527−534.

(24) Xiong, C.; Pernice, W.; Sun, X.; Schuck, C.; Fong, K.; Tang, H. *New J. Phys.* **2012**, *14*, 095014.
(25) Personal communication with Prof. Andrew Cleland's group, UC Santa Barbara.
(26) Hausmann, B. M.; Bulu, I.; Deotare, P. B.; McCutcheon, M. W.; Venkataraman, V.; Markham, M. L.; Twitchen, D. J.; Loncar, M. *Nano Lett.* **2013**, *13*, 1898−1902.
(27) Fiore, V.; Yang, Y.; Kuzyk, M. C.; Barbour, R.; Tian, L.; Wang, H. *Phys. Rev. Lett.* **2011**, *107*, 133601.
(28) Rosenberg, J.; Lin, Q.; Painter, O. *Nat. Photonics* **2009**, *3*, 478−483.
(29) Poot, M.; Fong, K. Y.; Bagheri, M.; Pernice, W. H. P.; Tang, H. X. *Phys. Rev. A* **2012**, *86*, 053826.